
PERGAMON

Journal of Quantitative Spectroscopy & Radiative Transfer 70 (2001) 569–579

Journal of Quantitative Spectroscopy & Radiative Transfer

www.elsevier.com/locate/jqsrt

Identification of cloud phase from PICASSO-CENA lidar depolarization: a multiple scattering sensitivity study

Yong-X. Hu[a,*], David Winker[a], Ping Yang[b], Bryan Baum[a], Lamont Poole[a], Lelia Vann[a]

[a] *NASA Langley Research Center, Radiation and Aerosol Branch, MS 420, Hampton, VA 23681, USA*
[b] *Code 913/SSAI, NASA GSFC, Greenbelt, MD, USA*

Abstract

A fast Monte Carlo simulation scheme is developed to assess the impact of multiple scattering on space-based lidar backscattering depolarization measurements. The specific application of our methodology is to determine cloud thermodynamic phase from satellite-based lidar depolarization measurements. Model results indicate that multiple scattering significantly depolarizes backscatter return from water clouds. Multiple scattering depolarization is less significant for non-spherical particles. There are sharp contrasts in the depolarization profile between a layer of spherical particles and a layer of non-spherical particles. Although it is not as obvious as ground-based lidar observations, it is likely that we can identify cloud phase not only for a uniform cloud layer, but also for overlapping cloud layers where one layer contains ice and the other water droplets.

1. Introduction

Numerous studies have reported on methods to infer cloud properties from passive radiometer measurements, such as from the moderate resolution imaging spectroradiometer (MODIS) instrument on the Earth observing system (EOS) Terra platform [1–3]. Infrared cloud properties include cloud height, cloud thermodynamic phase, optical thickness, and effective particle size. However, retrievals of the optical thickness and effective particle size depend critically on an accurate determination of the cloud thermodynamic phase. For many cases, such as an optically thick ice cloud residing at a height near the tropopause or a boundary layer water cloud, determination of cloud thermodynamic phase is relatively straightforward. There are many cases for

* Corresponding author. Tel.: +1-757-864-9824; fax: +1-757-864-7775.
E-mail address: y.hu@larc.nasa.gov (Y.-X. Hu).

0022-4073/01/$ - see front matter
PII: S0022-4073(01)00030-9

which accurate determination of cloud phase is problematic. For example, clouds at temperatures between 240 and 273 K may consist of supercooled water droplets or a mixture of supercooled droplets and ice crystals (i.e., mixed-phase clouds). Cloud phase determinations also become difficult when overlapping cloud layers are present. If the uppermost cloud layer is transmissive, like thin cirrus, the presence of a lower-level cloud layer can complicate the interpretation of satellite radiometer data.

For complex cloud scenes, there is room for improvement in the accuracy of cloud thermodynamic phase determined from satellite images. One way of evaluating the cloud phase from passive radiometry measurements is to compare with active sensors. Previous studies have shown the utility of a depolarization lidar to evaluate cloud phase. These studies have typically used either surface- or aircraft-based depolarization lidars to investigate this issue [4–9]. In this study, we investigate the use of a spaceborne depolarization lidar under development of launch on the PICASSO-CENA platform.

Most lasers generate linearly polarized radiation ($I_0 = Q_0,\ U_0 = V_0 = 0$). For spherical particles, such as water droplets, the single-scatter backscattering signals are minimally depolarized ($\delta = (I-Q)/(I+Q) = 0$ for 180° scattering angle) [10] at wavelengths where the hydrometeors have very little absorption. This is easily explained from the following equation:

$$\begin{pmatrix} I \\ Q \\ U \\ V \end{pmatrix} = \begin{pmatrix} P_{11} & P_{12} & 0 & 0 \\ P_{21} & P_{22} & 0 & 0 \\ 0 & 0 & P_{33} & P_{34} \\ 0 & 0 & P_{43} & P_{44} \end{pmatrix} \begin{pmatrix} I_0 \\ Q_0 \\ 0 \\ 0 \end{pmatrix}, \tag{1}$$

where I, Q, U, V are the elements of stokes vector and P_{ij} are the elements of the phase matrix. For spherical particles, the elements $P_{11} = P_{22}$ and $P_{12}(180^\circ) = P_{21}(180^\circ) = 0$. For scattering angles other than 180° and 0^0, P_{12} and P_{21} are not zero.

At backscattering angles, single-scattering from non-spherical particles such as ice crystals tends to depolarize. The degree to which the light depolarizes depends on particle shape, size and orientation [10,11]. The depolarization can be explained by looking at the properties of the scattering matrix at the backscattering angle, where $P_{11}(180^\circ) \neq P_{22}(180^\circ)$.

Because of the significant difference in single scattering depolarization, lidar backscattering depolarization measurements contain useful information for the determination of particle sphericity and thus may be employed to discriminate water clouds and ice clouds [12–16].

When the field of view is very small, single scattering dominates [9] in surface-based lidar measurements. However, backscattering signals from space-based lidar requires better assessment of multiple scattering effects, especially for relatively dense media such as clouds and thick aerosols. Multiple scattering effects increase as the field of view increases. For spherical particles, the multiple scattering will depolarize observed radiation in the backscattering direction.

In this study, we examine the potential of the PICASSO-CENA lidar [17] for the determination of cloud phase (ice, water, or a mixture of the two) from backscattering depolarization observations from space. We summarize a fast Monte Carlo simulation scheme in the next section and present sensitivity studies from model results in the section after.

2. Analytic fraction trace: a fast Monte Carlo simulation scheme

The statistical concept of our Monte Carlo scheme is similar to the ray tracing technique. Instead of tracing each photon to determine its path through the medium, we combine the ray tracing with several analytic estimates to speed up the convergence. Through this method, it is possible to determine for each photon a probability about whether it will enter the lidar receiver. The basic procedure of the scheme is as following:

For a group of photons with stokes vector (I_0, Q_0, U_0, V_0) and $Q_0 = I_0,\ U_0 = V_0 = 0$,

1. Find the location of next photon–particle interaction, using the equation: $\beta_e||\vec{r} - \vec{r}_0|| = -\ln(1-\xi)$. ξ is a random number with uniform distribution between 0 and 1. β_e is the extinction coefficient.
2. If the interaction is absorption, or if the location $\vec{r}$ is outside of the medium, start a new group of photons and go to step 8; if the interaction is scattering, proceed to the next step.
3. If the new location is inside the lidar field of view and within the medium, analytically estimate the probability that the photons will directly enter the lidar sensor without further interaction with the medium:

$$\begin{pmatrix} i \\ q \\ u \\ v \end{pmatrix} = \begin{pmatrix} I \\ Q \\ U \\ V \end{pmatrix} \omega \Delta\Omega_{\text{dish}} \exp\left(-\frac{\beta_e \Delta z}{\cos\theta_{\text{scat}}}\right), \tag{2}$$

$$\begin{pmatrix} I \\ Q \\ U \\ V \end{pmatrix} = L(\pi - \Phi_2) P(\Theta) L(-\Phi_1) \begin{pmatrix} I_0 \\ Q_0 \\ U_0 \\ V_0 \end{pmatrix}, \tag{3}$$

$$\cos\Phi_1 = \frac{\cos\theta_{\text{scat}} - \cos\theta_{\text{inc}}\cos\Theta}{\sin\theta_{\text{inc}}\sin\Theta}, \tag{4}$$

$$\cos\Phi_2 = \frac{\cos\theta_{\text{inc}} - \cos\theta_{\text{scat}}\cos\Theta}{\sin\theta_{\text{scat}}\sin\Theta}, \tag{5}$$

$$L(\Phi) = \begin{pmatrix} 1 & 0 & 0 & 0 \\ 0 & \cos 2\Phi & \sin 2\Phi & 0 \\ 0 & -\sin 2\Phi & \cos 2\Phi & 0 \\ 0 & 0 & 0 & 1 \end{pmatrix}. \tag{6}$$

Here Θ is the scattering angle, ω is the single scattering albedo, $\Delta\Omega_{\text{dish}}$ is the solid angle viewing the lidar aperture from the location of the photon–particle interaction, and ϕ_{inc} and

θ_{inc} are the azimuth angle and viewing zenith angle of the incident light, respectively. The quantities ϕ_{scat} and θ_{scat} are the azimuth angle and viewing zenith angle of the scattered light, respectively, which is based on the satellite viewing geometry of the location $\vec{r}$. Δz is the vertical distance between the location and the top of the scattering medium. Φ_1 is the angle between the incoming light plane and the scattering plane, and Φ_2 is the angle between the outgoing light plane and scattering plane [18]. $P(\Theta)$ is the phase matrix, and L is the rotation matrix.

There are special cases where Eqs. (4) and (5) are singular. When $\sin\Theta = 0$, Eqs. (4) and (5) are replaced by

$$\cos\Phi_1 = 1, \quad \cos\Phi_2 = 1. \tag{7}$$

When $\sin\theta_{\text{inc}} = 0$, Eqs. (4) and (5) are replaced by

$$\cos\Phi_1 = -\cos\theta_{\text{inc}}\cos(\phi_{\text{scat}} - \phi_{\text{inc}}), \quad \cos\Phi_2 = \cos\theta_{\text{inc}}. \tag{8}$$

When $\sin\theta_{\text{scat}} = 0$, Eqs. (4) and (5) are replaced by

$$\cos\Phi_2 = -\cos\theta_{\text{scat}}\cos(\phi_{\text{scat}} - \phi_{\text{inc}}), \quad \cos\Phi_1 = \cos\theta_{\text{scat}}. \tag{9}$$

4. Rotate the coordinate to laser polarization reference coordinate and add i, q to the lidar signal. Steps 3 and 4 are our analytic procedures. For each scattering process, as long as there are enough photons, there is a certain probability of photon scattering directly into the receiver without further interaction. Calculating this probability analytically significantly reduces the computational requirements relative to a pure Monto Carlo approach [19–21].
5. Now come back to normal Monte Carlo ray tracing. First, determine the scattering angle Θ and relative azimuth angle ϕ_r based upon phase function P_{11}, then determine the new scattering direction μ and ϕ.

   Θ is calculated from the accumulative probability of the phase function $F(\cos\Theta) = \int_0^{\cos\Theta} P_{11}(\theta)\,\mathrm{d}\cos\theta$ as following:

$$\Theta = \cos^{-1} F^{-1}(\xi_1), \quad \phi_r = 2\pi\xi_2. \tag{10}$$

   Here ξ_1 and ξ_2 are random numbers with uniform distribution from 0 to 1.

   μ and ϕ are calculated from

$$\mu = \mu_0 \cos\Theta + \sqrt{(1-\mu_0^2)(1-\cos^2\Theta)}\cos\phi_r, \tag{11}$$

$$\phi = \phi_0 + \cos^{-1}\frac{\cos\Theta - \mu_0\mu}{\sqrt{(1-\mu^2)(1-\mu_0^2)}}. \tag{12}$$

6. Modify the probability of the photon scattering toward direction (μ, ϕ) by considering the state of polarization:

$$\begin{pmatrix} I \\ Q \\ U \\ V \end{pmatrix} = L(\pi - \Phi_2) \begin{pmatrix} 1 & \frac{P_{12}}{P_{11}} & \frac{P_{13}}{P_{11}} & \frac{P_{14}}{P_{11}} \\ \frac{P_{21}}{P_{11}} & \frac{P_{22}}{P_{11}} & \frac{P_{23}}{P_{11}} & \frac{P_{24}}{P_{11}} \\ \frac{P_{31}}{P_{11}} & \frac{P_{32}}{P_{11}} & \frac{P_{33}}{P_{11}} & \frac{P_{34}}{P_{11}} \\ \frac{P_{41}}{P_{11}} & \frac{P_{42}}{P_{11}} & \frac{P_{43}}{P_{11}} & \frac{P_{44}}{P_{11}} \end{pmatrix} L(-\Phi_1) \begin{pmatrix} I_0 \\ Q_0 \\ U_0 \\ V_0 \end{pmatrix}, \tag{13}$$

where P_{ij} are the elements of the phase matrix, $L(\Phi_1)$ and $L(\Phi_2)$ have the same definition as the elements in Eq. (3).

With enough photons, this procedure yields the same results as for a more conventional Monte Carlo application which involves a more complicated multi-dimensional linear inverse mapping procedure that is very time consuming.

7. Replace stokes vector (I_0, Q_0, U_0, V_0) by (I, Q, U, V) from Eq. (13) and return to step 1 until the group of photons either exit the medium or are absorbed.
8. Start a new group of photons and return to step 1 until the backscattering signals converge.

The depolarization parameter δ is determined from a simulated backscattering stokes vector (i, q, u, v):

$$\delta = \frac{i - q}{i + q}. \tag{14}$$

The intensities calculated from the vector model compare very well with the those from previous scalar Monte Carlo multiple scattering models [21,22].

The Monte Carlo scheme described above can speed up model convergence significantly. Most photons do not reach the receiver. The chances of a transmitted photon returning to the PICASSO lidar receiver is less than 1 in 10 billion for typical water clouds. The odds of a photon entering the PICASSO lidar receiver decrease as the optical thickness of the medium decreases. Conventional Monte Carlo methods are typically straightforward to implement. However, for space-borne lidar simulation, the speed will be a problem because only a single detection produced from more than 10^{10} transmitted photons. After N photons are emitted and traced, the rms error of result is proportional to

$$\Delta I_{\text{err}} = \pm \frac{\sigma_1}{\sqrt{N \times 10^{-10}}}, \tag{15}$$

where σ_1 is the standard deviation.

The analytic method derived above generates n readings for each photon, where n is the average number of photon–medium interactions inside the lidar field of view before the photon eventually leaves the medium. After N photons are traced, the rms error of model result is

$$\Delta I_{\text{err}} = \pm \frac{\sigma_2}{\sqrt{n \times N}}. \tag{16}$$

Here the standard deviation σ_2 is about one order of magnitude smaller than σ_1, depending on the single scattering properties of the medium and total cloud optical thicknesses. The analytic method is at least 10^5 faster than conventional Monte Carlo methods with convergence to the same accuracy.

To explain why the results of this method are exactly the same as a conventional Monte Carlo method, we now consider a simplified case to illustrate the logic of the analytic scheme.

Consider a photon traveling in a special non-absorbing scattering medium as follows:

For each photon entering the medium, the photon is provided three choices for each scattering interaction: (A) stay inside the medium (probability a) and perhaps undergo multiple scattering events; (B) leave the medium, but do not enter the receiver (probability b); (C) scatter directly into the receiver (probability c);

$a+b+c=1$. If a conventional Monte Carlo procedure is not flawed, the probability of photon reaching the lidar receiver after multiple scattering is

$$P_c = \frac{c}{b+c}. \tag{17}$$

Application of the analytic approaches in our Monte Carlo scheme will produce results as

$$\begin{aligned} P_c &= c + ac + \cdots + a^{k-1}c + \cdots \\ &= \frac{c}{b+c}, \end{aligned} \tag{18}$$

where the kth term of the right hand side is the probability of photon scattering k times (a^{k-1}, which is the objectives of steps 5 and 6) multiples the probability the photon reaches the receiver directly without further interaction (c, which is the objectives of steps 3 and 4).

Although the real model is much more complicated, the fundamentals are the same.

3. Model results

This study simulates depolarization of PICASSO-CENA Lidar backscattering at a 532 nm wavelength. The receiver has a 0.13 mrad field of view (FOV). For an anticipated satellite altitude of 705 km, the diameter of the footprint is anticipated to be approximately 91 m. For simplicity, we assume that the laser transmitter has a zero divergence.

The phase matrix for spherical particles are computed from Mie theory. We assume a Gamma distribution to describe the particle sizes with a prescribed more radius and a 10% dispersion.

The improved geometric optics method (IGOM) [23] is used to calculate the scattering properties of four types of ice crystals: aggregates, hexagonal columns, bullet rosettes with moderate surface roughness, and bullet rosettes with smooth surfaces. In principle, in IGOM the ray tracing technique is employed to calculate the near field on particle surface with inclusion of complete phase information for the electric field. Subsequently, a rigorous electromagnetic integral equation is applied to map the near field to far field that can then be used to calculate single scattering properties. The procedures to define the three-dimensional geometry for the ice crystals and the surface roughness have been reported previously [24].

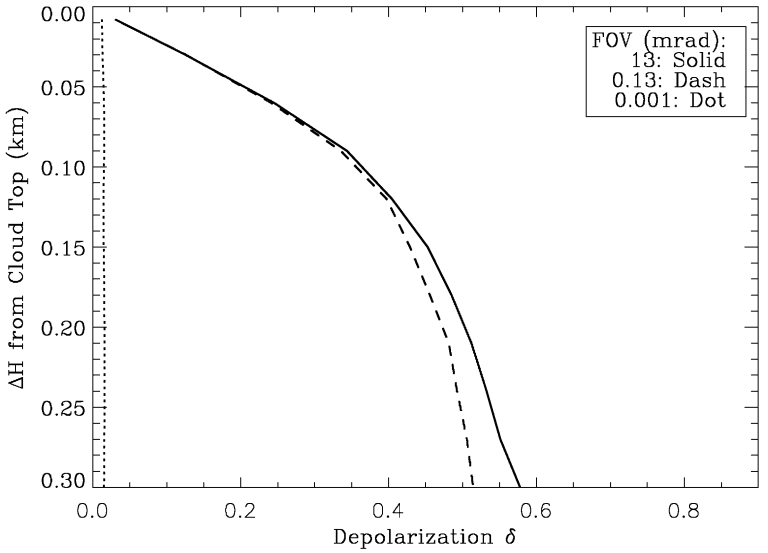

Fig. 1. Depolarization profiles for various FOV; here the medium is a water cloud layer with $\tau = 4$, $\mathrm{Re} = 6\ \mu\mathrm{m}$ and physical thickness 300 m.

For backscattering signals dominated by single scattering, since $I_0 = Q_0$, $P_{12} = P_{21}$, the depolarization can be expressed by

$$\delta = \frac{P_{11} - P_{22}}{P_{11} + P_{22}}. \tag{19}$$

For spherical particles, $P_{11}(180^\circ) = P_{22}(180^\circ)$ and thus there is no depolarization ($\delta = 0$). This is not the case for non-spherical particles. For typical non-spherical cloud particles, values of $\delta = 0$ as derived from the above equation range from 0.4 to 0.6. Based on this, we can identify water and ice clouds from lidar depolarization signals.

Lidar instruments with different FOV have different multiple scattering impacts [22]. A reduction in the lidar field of view will reduce the impact of multiple scattering. But there are trade offs because it also reduces the magnitude of the signal and thus reduces the instrument sensitivity. Fig. 1 shows that in a water cloud, the lidar backscattering signal becomes depolarized gradually due to multiple scattering as the pulse moves from cloud top toward the base of the water cloud layer. The slope of the depolarization decreases with decreasing FOV, since multiple scattering for a smaller field of view contributes relatively less toward the total backscattering signal.

As opposed to our results for spherical water droplets, multiple scattering plays a less important role in the depolarization from non-spherical ice particles (see Fig. 2). The δ value varies less than a few percent from the region dominated by single scattering (top of the cloud layer) to the region dominated by multiple scattering (bottom of the cloud layer).

The depolarization profiles vary for different ice particle shapes (see Fig. 2), but the difference is due primarily to differences in the single scattering δ. The depolarization profiles display little sensitivity to particle size (Fig. 3) for particles with rough surfaces, except for very small

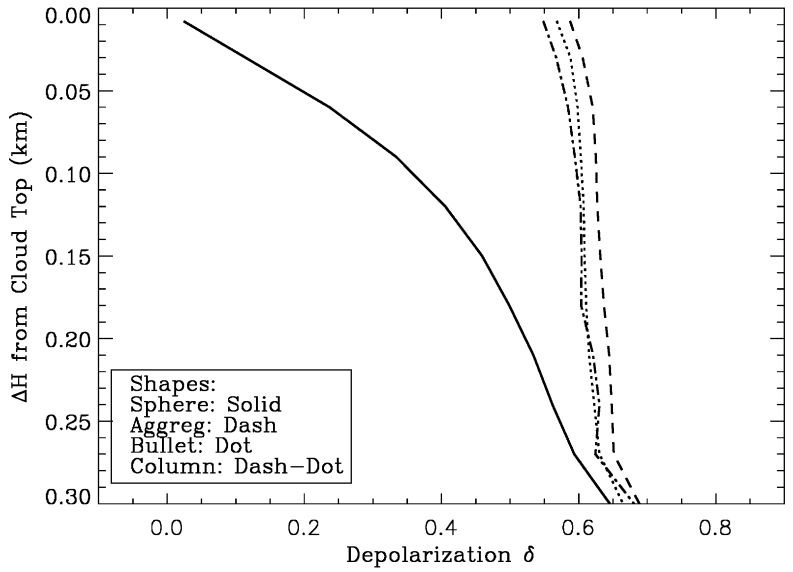

Fig. 2. Depolarization profile differences between spherical particles and non-spherical particles with different shapes. The optical depth of the medium is 4 and the physical thickness is 300 m.

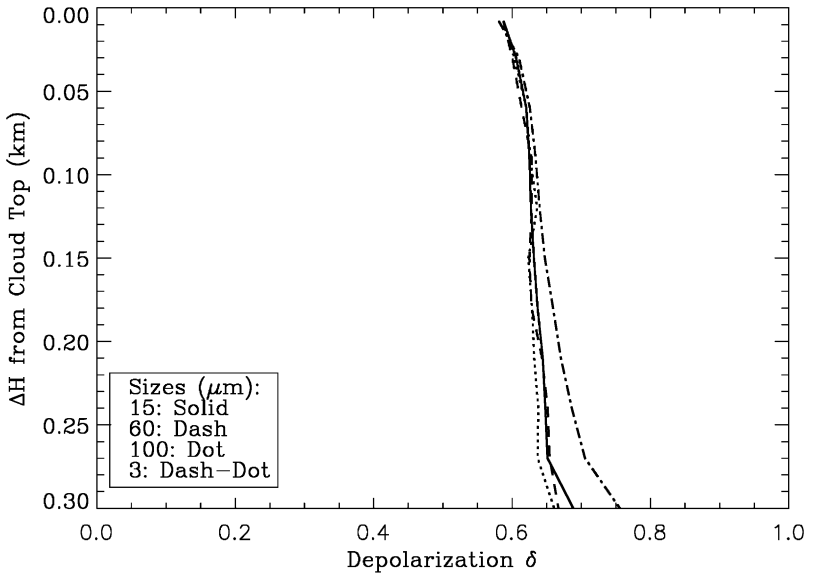

Fig. 3. Depolarization profile differences for non-spherical particles with the same shape but different maximum dimensions (sizes). The optical depth of the medium is 4 and the physical thickness is 300 m.

particles. For small particles with smooth surfaces, depolarization is very sensitive to the size parameter [25] and such sensitivities are used for separating different types of PSCs [26].

Multiple scattering tends to depolarize backscattering signals from spherical particles and may create difficulties in identifying cloud phase for overlapping cloud layers. Fig. 4 indicates the

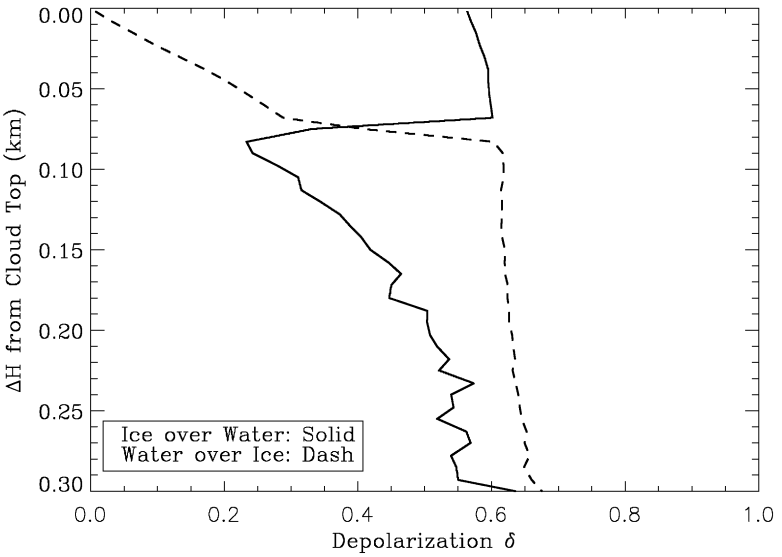

Fig. 4. Depolarization profile differences for two types of overlapping clouds (ice over water, water over ice). The optical thickness of the upper layer is 1 and the physical thickness is 75 m. The optical thickness of the bottom layer is 3 and the physical thickness is 225 m.

possibility of discriminating a layer of spherical particles overlaying a layer of non-spherical particles, if we compare the discontinuities and slopes of every piece of a depolarization profile. The value of δ for a layer of water cloud particles initially has a small value that increases gradually with distance through the cloud, while for a layer of ice particles, δ starts at a relatively large value that increases more slowly toward cloud base.

4. Summary

Ground-based lidar backscattering depolarization signals have been shown to contain useful information about particle sphericity and thus help to identity cloud phase (water and ice). This sensitivity study is a first step toward answering the question: can space-based lidar backscattering depolarization information also be used to identify cloud phase.

To answer this question, a Monte Carlo simulation scheme is proposed that incorporates various analytical techniques to increase convergence speed.

Results of this study of the PICASSO-CENA satellite Lidar are

- For spherical particles, such as water cloud droplets, the backscattering signal gradually depolarizes toward cloud base because of a multiple scattering effect. The effect is very different from ground-based lidar, for which the field of view are small and multiple scattering effects are relatively less important.
- For non-spherical ice cloud particles, most of the depolarization comes from single scattering. Multiple scattering causes the depolarization to increase toward cloud base more slowly than for water cloud layers.

- Depolarization for ice cloud is more sensitive to particle shapes than particle sizes.
- By studying the discontinuities and the slopes of depolarization profiles, it is possible to identify overlapping clouds containing opposite thermodynamic phases (i.e., where one layer is ice, the other water) and estimate particle sphericity within each layer.

One assumption employed in this study is that spherical particles are likely to be indicative of water clouds while non-spherical particles are indicative of ice clouds. For some cases, such as dense smoke and dust layers, this might lead to an incorrect conclusion, because that aerosol particles are not always spherical. Additional theoretical studies of absorbing aerosols and smokes are in progress. Other information, such as the ratio of 532 and 1064 nm backscatter, measurements from passive remote sensing instruments, and in situ measurements, are needed to reduce the ambiguities of determination.

The purpose of this study has been to investigate the effect of multiple scattering on the depolarization of lidar backscattering, which we anticipate will be significant for space-borne lidar measurements of cloud layers. More modeling simulations are needed, including testing the code for various types of scattering mediums, comparisons with other observations, and intercomparisons with other similar models.

Acknowledgements

This study was supported by PICASSO-CENA project. We would like to thank the anonymous reviewers for their suggestions.

References

[1] Baum BA, Soulen PF, Strabala KI, King MD, Ackerman SA, Menzel WP, Yang P. Remote sensing of cloud properties using MODIS Airborne Simulator imagery during SUCCESS. II. Cloud thermodynamic phase. J Geophys Res 2000;105:11781–92.
[2] Frey RA, Baum BA, Menzel WP, Ackerman SA, Moeller CC, Spinhirne JD. A comparison of cloud top heights computed from airborne lidar and MAS radiance data using CO2 slicing. J Geophys Res 1999;104:24547–55.
[3] Ackerman SA, Strabala KI, Menzel WP, Frey RA, Moeller CC, Gumley LI. Discriminating clear-sky from clouds with MODIS. J Geophys Res 1998;103:32141–58.
[4] Ferrare RA et al. Comparisons of LASE, aircraft, and satellite measurements of aerosol optical properties and water vapor during TARFOX. J Geophys Res 2000;105:9935–47.
[5] Moore AS et al. Development of the lidar atmospheric sensing experiment (LASE)—an advanced airborne DIAL instrument. Advances in atmospheric remote sensing with lidar. New York: Springer; 1997.
[6] Pal S, Carswell A. Polarization properties of lidar backscattering from clouds. Appl Opt 1973;12:1530–5.
[7] Sassen K, Petrilla R. Lidar depolarization from multiple scattering in marine stratus clouds. Appl Opt 1986;25:1450–9.
[8] Weinman J, Shipley S. Effects of multiple scattering on laser pulses transmitted through clouds. J Geophys Res 1972;77:7123–8.
[9] Sassen K, Chen T. Lidar dark band: an oddity of the radar bright band analogy. Geophys Res Lett 1995;22:3503–8.
[10] Sassen K. Lidar backscattering depolarization technique for cloud and aerosol research. Light scattering by non-spherical particles. New York: Academic Press; 1999. p. 393–416.

[11] Mishchenko MI, Hovenier JW. Depolarization of light backscattering by randomly oriented non-spherical particles. Opt Lett 1995;20:1356–8.
[12] Liou K-N, Lahore H. Laser sensing of cloud composition: a backscatter depolarization technique. J Appl Meteor 1974;13:257–63.
[13] Sassen K. The polarization lidar technique for cloud research: a review and current assessment. Bull Amer Meteor Soc 1991;72:1848–66.
[14] Platt CMR, Scott JC, Dilley AC. Remote sensing of high clouds. Part VI: optical properties of midlatitude and tropical cirrus. J Atmos Sci 1987;44:729–47.
[15] Eloranta EW, Piironen P. Measurements of cirrus cloud optical properties with the University of Wisconsin high spectral resolution lidar. Advances in atmospheric remote sensing with lidar. Berlin: Springer; 1996.
[16] Piironen P. A high spectral resolution lidar based on an iodine absorption filter. Thesis, Univ. Wisconsin, 1994.
[17] Winker D, Wielicki B. The PICASSO-CENA Mission. Sensors, systems and next-generation satellites III, Proceedings of SPIE, Vol. 3870, 1999. p. 26–36.
[18] Hovenier J, Mackowski D. Fundamental relationships relevant to the transfer of polarized light in a scattering atmosphere. Astron Astrophys 1983;128:1–16.
[19] Poole LR, Venable DD, Campbell JW. Semianalytic Monte Carlo radiative transfer model for oceanographic Lidar systems. Appl Opt 1981;20:3653–6.
[20] Winker DM, Osborne MT. Preliminary analysis of observations of the pinatubo volcanic plume with a polarization—sensitive lidar. Geophys Res Lett 1992;19:171–4.
[21] Winker D, Poole L. Monte Carlo calculations of cloud returns for ground-based and space-based lidars. Appl Phys B 1995;60:341–4.
[22] Eloranta EW. A practical model for the calculation of multiply scattered lidar returns. Appl Opt 1998;37: 2464–72.
[23] Yang P, Liou KN. Geometric-optics-integral-equation method for light scattering by non-spherical ice crystals. Appl Opt 1996;35:6568–84.
[24] Yang P, Liou KN. Single-scattering properties of complex ice crystals in terrestrial atmosphere. Control Atmos Phys/Beitr Phys Atmos 1998;71:223–48.
[25] Mishchenko MI, Sassen K. Depolarization of lidar returns by small ice crystals: an application to contrails. Geophys Res Lett 1998;25:309–12.
[26] Poole L, Kent G, McCormick P. Dual-polarization lidar observations of polar stratospheric clouds. Geophys Res Lett 1990;17:389–92.